DYNAMIC LOCAL DISTENSIBILITY OF LIVING ARTERIES AND ITS RELATION TO WAVE TRANSMISSION

JAN BAAN, JAN P. SZIDON, *and* ABRAHAM NOORDERGRAAF

From the Cardiovascular-Pulmonary Division, Department of Medicine, and the Bio-Engineering Department, Moore School of Electrical Engineering, University of Pennsylvania, Philadelphia, Pennsylvania 19104

ABSTRACT The dynamic local distensibility of the abdominal aorta was measured in 11 anesthetized dogs by recording simultaneously phasic pressure and instantaneous intravascular cross-sectional area, utilizing a special transducer. Axial motion of the vessel wall was recorded using a modification of the same transducer. A nonlinear relationship was found to exist between area and pressure in most cases studied. Fourier analysis was performed on data from eight experiments in order to obtain frequency characteristics of distensibility. In roughly half of the cases, Fourier analysis revealed that pressure variations displayed a phase lead over area variations for frequencies up to 10 Hz. This phenomenon was ascribed to viscoelastic properties of the vessel wall and the magnitude of the phase leads roughly matched those found in vitro by others. The behavior of the vessel wall in these instances was correctly predicted by the dynamic formula for distensibility, derived by others from wave transmission theory in which absence of axial wall motion is assumed. In these experiments, axial motion of the wall was found to be virtually absent. In the other half of the cases, the reverse situation was obtained: a phase lead of area variations over pressure variations for frequencies up to 15 Hz. In those cases a craniocaudal axial displacement of the vessel wall was observed with each systole, amounting to around 1 mm. The finding of the phase leads was partially explained by a dynamic formula for distensibility, developed by us from the theory of wave transmission in which free axial motion of the wall is a chosen boundary condition. The sign and order of magnitude of the phase leads were correctly predicted by the theoretical formula, but there was a disagreement on the frequency range in which they occurred. We concluded that additional forces, not yet considered in theoretical treatments, are operative on the aortic wall, which account for this lack of agreement. The frequency dependent properties of distensibility in vivo cannot be compared to those obtained in vitro in those cases in which there is axial displacement of the vessel wall of the same order of magnitude as the radial extensions.

INTRODUCTION

The present study of the dynamic local distensibility of arteries was undertaken in view of the importance of this variable in the behavior of the arterial tree as a wave

transmission system. In addition, we checked whether the dynamic measurement of distensibility in vivo gave results which could be compared to the dynamic viscoelastic properties of the vessel wall obtained in vitro by other investigators.

The distensibility of a segment of artery is defined as the increase in volume per unit increase in transmural pressure. Because of cylindrical symmetry, volume has two components: axial (i.e. length) and radial (i.e., radius, diameter, circumference, or cross-sectional area). Under the circumstances prevailing in a study in vitro, the segment is closed at both ends while pressure is the only driving force. If the wall material is considered isotropic and incompressible (Poisson's ratio = 0.5 [1]), no changes in segment length will occur so that the only variable changing with pressure is the radial component (Love, pp. 144–145 [2]). Local vessel distensibility per unit length may then be defined as dS/dP, where dS is the increment in cross-sectional area S and dP is the increment in pressure P. In a study in vivo, not all of the above conditions are met and the definition of distensibility will have to be broadened as discussed below.

Arterial distensibility has been studied in vivo by many investigators with various techniques (external circumference [3–5], external diameter [6–15], internal diameter [16–22], or internal cross-sectional area [23, 24]). These studies in vivo were sometimes predated by studies in vitro (25–27), while some investigators obtained data under both circumstances (3, 4, 10, 28, 29). Whenever variations in the radial component are in phase with variations in the pressure, the wall material is characterized as purely elastic. When the variations in the radial component display a phase lag behind the variations in pressure, the wall material is viscoelastic. In general, this phenomenon can be described quantitatively by the values of the elastic and the viscous component of the wall's complex Young's modulus, which have both been found to be frequency dependent (6, 12, 19, 27). However, with measurements in the living system, a phase lead of the variations in the radial component over the variations in pressure was also frequently observed (3, 4, 9, 10, 12, 23, 24, 30). The mechanism of this latter phenomenon has been poorly understood and has been tentatively attributed either to instrument error (4, 9), wall muscle activity (4), or to changes in segment length (31, 32). A more complete understanding of the mechanism might be gained by relating the quantity arterial distensibility to the theoretical treatment of wave transmission through the arterial tree since the latter has reached a high level of sophistication (33).

WAVE TRANSMISSION

In the description of the arterial circulation as a wave transmission system, the heart is considered to be a wave generator, linked to the periphery via an extensive set of short vessel segments undergoing multiple branching (33–38). In analogy with transmission line theory, each vessel segment is fully characterized by a set of three quantities: (*a*) Longitudinal fluid impedance per unit length, Z_l, defined per har-

monic as the ratio of pressure gradient, $-dP/dz$, over pulsatile flow, dQ; (z = longitudinal coordinate). (*b*) Transverse wall admittance per unit length, Y_t, defined per harmonic as the ratio of flow gradient, $-dQ/dz$, over pulsatile pressure, dP. Transverse impedance $Z_t = 1/Y_t$. (*c*) Segment length, L.

The pressure-flow relationship in such a segment is then fully characterized by one more quantity: (*d*) Input impedance, Z_i, defined per harmonic as the ratio of pressure, P, over flow, Q, at the entrance of the segment. (Load impedance could have been chosen instead).

Theory and measurement of longitudinal fluid impedance, introduced by Womersley (39), have received wide attention since Witzig's original contribution (40). They will not be a subject of further discussion in this study. In contrast, the concept of transverse wall impedance, introduced by Jager et al. (34) has not yet become as popular, probably because most investigators of vessel distensibility and elasticity failed to relate their findings to wave transmission phenomena. Nevertheless, the two impedances Z_i and Z_t have equal importance in defining the transmission of pressure and flow waves in the arterial tree, which can be appropriately described by such quantities as characteristic impedance Z_0 ($= \sqrt{Z_i Z_t}$), propagation constant $\gamma(= \sqrt{Z_i Z_t})$, load impedance and reflection coefficient (Westerhof et al., [38]). All of the above quantities are complex and frequency dependent and thus we have for, e.g., the propagation constant:

$$\gamma(\omega) = \alpha(\omega) + j\beta(\omega), \tag{1}$$

in which α determines the wave attenuation and β the phase velocity c (ω = angular frequency):

$$c(\omega) = \omega/\beta(\omega). \tag{2}$$

It is precisely in the definition of transverse impedance that the importance of local vessel distensibility resides. Namely, for a vessel segment of cross-sectional area S (not necessarily circular) and infinitesimal length dz, through which the flow of incompressible fluid is Q, the net increase in volume per unit time (t) and per unit length can be expressed as $-dQ/dz$ on the one hand and as dS/dt on the other. Thus we have:

$$-dQ/dz = dS/dt. \tag{3}$$

For the harmonic of S with angular frequency ω we have:

$$dS/dt = j\omega\, dS, \tag{4}$$

and so we can write:

$$Y_t = (-dQ/dz)/dp = j\omega(dS/dP), \tag{5}$$

or:

$$Z_t = (1/j\omega)(dP/dS). \tag{6}$$

Thus, the transverse wall impedance is inversely proportional to local vessel distensibility per unit length. This holds true also for random geometries such as veins. (The above relation [Eq. 3] can also be derived by radial integration of the differential equation of continuity for the incompressible fluid [23]).

Theoretical solutions for the longitudinal and transverse impedance (and thus for the derived quantities dS/dP, Z_0, γ, etc.) in their most sophisticated form derive from the linearized constitutive equations for viscous oscillatory flow in thick-walled, viscoelastic, circular vessel segments, of homogeneous and isotropic material, with the proper boundary conditions imposed (Navier-Stokes equation for the fluid; Navier equation for the wall). The solutions differ depending on which boundary condition is chosen for the axial motion of the vessel wall. Relevant to this study are only the formulas derived for dS/dP. The two different boundary conditions for the wall motion, with the two different solutions are:

(*a*) The wall, although free to move in radial direction, is completely restricted from moving in axial direction by infinitely strong axial tethering to the perivascular tissue. The solution for the distensibility in that case is (38):

$$(dS/dP)(\omega) = [3\pi a^2(1 + h)^2]/[E^*(\omega)h(2 + h)], \tag{7}$$

in which $E^*(\omega)$ = complex Young's modulus, a = internal radius, h = ratio of wall thickness over radius a. Interestingly, this formula, derived by Jager (35) from the very complex dynamic equations for the first time, is essentially the same as that derived for the static case in, e.g., Love, p. 144 (2).

(*b*) The vessel wall is completely free to move in radial as well as axial direction, driven by pressure and viscous drag of the blood flow, unrestricted by perivascular tissue. This case has not been solved for completely in the past. Numerical solutions for Z_t and γ were given by Cox (41). An analytical solution for γ was given by Baan (23). Employing the same approximations as those used to find γ, the following formula was derived[1] for the distensibility:

$$\frac{dS}{dP}(\omega) = \frac{3\pi a^2(1 + h)^2}{E^*(\omega)h(2 + h)}\, g(F_{10}) \left\{1 - F_{10}\, \frac{\omega^2 g(F_{10})(2 + 2h - a^2 h) - 6jh}{\omega^2 g(F_{10})(2 + 2h - a^2 F_{10}\, h)}\right\}, \tag{8}$$

in which:

$$g(F_{10}) = \frac{4 - F_{10} + \{(4 - F_{10})^2 - 12[h(2 + h)/(1 + h)^2] \cdot (1 - F_{10})(1 - [F_{10}/h(2 + h)])\}^{1/2}}{6(1 - F_{10})}, \tag{9}$$

[1] Baan, J. Manuscript in preparation.

$F_{10} = 2J_1(\alpha_w j^{3/2})/\alpha_w j^{3/2} J_0(\alpha_w j^{3/2})$, $\alpha_w = a\sqrt{\omega/\nu}$ (Womersley [39]), ν = kinematic fluid viscosity, J_0 and J_1 are Bessel functions or order 0 and 1, respectively.

Note that the formula (Eq. 8) is for the complex dynamic case and has as yet no explicit counterpart in the static case since the axial wall stress (Love, [2]) is hard to define. Womersley (42) has given solutions for the similar (i.e. untethered), but much simpler dynamic case of a purely elastic, thin-walled tube. The importance of Eqs. 7 and 8 will be elaborated upon in the discussion section. It should be noted here that, if anisotropy and inhomogeneity of the wall were present (47), the theoretical treatment would become even more complex should these properties be taken into account.

In view of the above theoretical considerations, it seemed appropriate to detect axial motion (if any) of the vessel wall, in addition to recording dynamic pressure and dynamic cross-sectional area, when measuring arterial distensibility in vivo. Furthermore, before a valid comparison between theory and experiment can be made, it should be remembered that theoretical treatments so far have largely been linear. Therefore, if a nonlinear relation between pressure and radial dimension is found (6, 9, 11, 12, 19, 26), this effect should be corrected for. Namely, if two dynamic quantities are in phase but related to one another in even a slightly nonlinear fashion, and their ratio is plotted against frequency (after Fourier analysis), a marked phase angle, dependent on frequency, results (Gow and Taylor [12]). Consequently, it was deemed necessary to try and remove the nonlinearity effectively from the data whenever present.

METHODS

Phasic intravascular cross-sectional area and pressure at the same site were recorded in the abdominal aorta of 11 mongrel dogs, weighing from 22 to 31 kg, anesthetized with intravenous 5% chloralose in propylene glycol (100 mg/kg body mass). After exposing the sacral artery via a low abdominal incision, an intravascular area transducer was advanced into the distal abdominal aorta and positioned about 8 cm cranial to the bifurcation. This location was essentially free from side branches (not counting miniature branches smaller than 1 mm in diameter). Since the technique does not require dissection of the vessel segment under investigation, the axial tethering as well as the nervous supply was usually left intact. In two experiments, moderate dissection of the aorta was performed about 2 cm distal from the site of distensibility measurement, while miniature branches were ligated in order to facilitate the positioning of a flow probe.

Area Measurement

The intravascular area transducer employed has been described in detail elsewhere (23, 24). In essence, a homogeneous, alternating magnetic field was applied parallel to the vessel axis, utilizing a pair of coils around the body. The transducer consisted of a pick-up loop which was placed inside the vessel perpendicular to the magnetic field. The rectified voltage induced by the field in the pick-up loop was linearly proportional to the instantaneous cross-sectional area. The transducer loop was constructed in such a way that it could be folded on the tip of a pressure catheter, protected by a gelatin capsule while the catheter was intro-

duced. When the catheter was in place, the capsule melted and dissolved, allowing the transducer loop to unfold and position itself against the vessel wall, whose motion it then followed by spring action. Loading of the wall was negligibly small and blood flow was unobstructed. The transducer also incorporated a very small, multiple turn reference coil of known, fixed area, with its axis parallel to the vessel's axis. It served for in vivo calibration of the area signal and was also used to detect axial motion of the vessel wall as described below.

Frequency characteristics of the area transducer were obtained by a specially built test rig (24). The amplitude characteristic was flat from 0–30 Hz; the phase characteristic displayed a lag increasing linearly with frequency by 0.4° per Hz.

Axial Motion Detection

The procedure to detect axial or longitudinal motion of the vessel wall consisted in changing the position of the pair of extracorporeal coils in such a way as to produce a very inhomogeneous magnetic field at the site of measurement. As the transducer—being very light (0.06 g), sitting snugly against the wall, while being connected to the outside with very flexible wiring—moved with the vessel wall in an axial direction, the fixed area reference coil cut through varying magnetic field strengths, thus varying its induced voltage. Over the small range of motion encountered (a few millimeters maximally) this signal was linear. Calibration of the signal was obtained by moving a second reference coil of equal cross-sectional area over a known axial distance outside the vessel as close as possible to the site of measurement. The resolution of the technique was about 0.2 mm, limited by the recorder's line thickness and equipment noise. The method did not allow for the recording of axial and radial motion of the vessel wall simultaneously.

Pressure Measurement

Phasic intravascular pressure was measured using a short (10 cm) Fr. no. 6 saline-filled catheter connected to a Statham P23Db strain gauge transducer (Statham Instruments, Inc., Oxnard, Calif.). The catheter had a lateral hole coinciding with the center of the area transducer. The frequency response of the catheter-manometer system was flat in amplitude from 0–7.5 Hz with an overshoot increasing linearly with frequency above 7.5 Hz by 0.4% per Hz, while displaying a phase lag increasing linearly with frequency by 0.125° per Hz. Respiratory movements were recorded with a pneumograph. Blood flow measurements were taken in only two experiments and are not a part of this study.

Data Recording and Analysis

The phasic signals of area, pressure, and axial motion were inscribed at maximal gain on an optical recorder (Electronics for Medicine [White Plains, N. Y.] model DR-12) at high paper speeds (100–200 mm/s). In addition, vector plots of area vs. pressure were obtained using the *X-Y* plotter of the recorder. In eight experiments the tracings were optically enlarged by about a factor 10 and retraced on millimeter paper, thus filtering out noise. Only heart cycles obtained during expiratory pause were analyzed because systolic and diastolic area and pressure levels tended to be fairly steady during this period, while heart rate is also more constant; moreover, axial vessel motion was always minimal during expiratory pause (see below). On the average, 10 heartbeats were analyzed per experiment. In digitizing the phasic signals, the diastolic values at the beginning and end of each cycle were assumed equal, a procedure necessary for proper frequency analysis if one is interested only in the heart frequency and its harmonics. Digital samples from the enlarged tracings were taken at the rate of 50–80

samples per cycle and fed into a PDP-9 computer (Digital Equipment Corp., Maynard, Mass.), which was programmed to calculate the first 12 harmonics of area and pressure by Fourier analysis. The frequency components were then corrected by a subroutine for the small frequency dependent errors of the instruments as specified above. The resulting corrected frequency components were fed into an IBM 360/75 computer which resynthetized the data into the time domain and printed out vector plots of area vs. pressure using a Calcomp plotter (California Computer Products, Anaheim, Calif.). These plots were used to approximate the nonlinear relationship between area and pressure after which the nonlinearity was removed by the technique described below. The resulting phasic "linearized" pressure (P') and area (S) data were reentered into the PDP-9 computer to obtain their frequency components by Fourier analysis. From these, the frequency characteristics of the linearized inverse distensibility, dP'/dS, resulted: its modulus $|P'/S|$ (normalized to 1.0 at zero frequency), defined as the ratio of the moduli of the linearized pressure, $|P'|$, and of area, $|S|$, and its phase angle, $\Delta\phi$, defined as the difference of the phase angles of linearized pressure, $\phi_{P'}$, and of area, ϕ_S.

Linearization Procedure

At the mean pressure levels prevailing (ranging from 120 to 170 mm Hg), most of the vector plots of area vs. pressure displayed nonlinearity (Fig. 1 *a*). In order to eliminate the effect of nonlinearity, the following procedure was used. The coordinates of the points A (bottom), B (top), and C (center) of the vector loop produced by the Calcomp plotter were determined (i.e. after correction for instrument errors). The point C was chosen on the midline of the line connecting A and B, half-way between the upstroke and downstroke of the vector loop (Fig. 1). The quadratic curve, described by:

$$P' = kP^2 + lP + m, \tag{10}$$

which fitted through the points A, B, and C, was determined by computer-solving for the constants k, l, and m. This curve, shown as the dashed line in Fig. 1 *a*, was considered to represent the purely nonlinear area-pressure relationship, exhibiting constant modulus ratio and zero phase difference at all frequencies. In the final frequency analysis, the original pressure sample points (P) were replaced by the corresponding P' points obtained from Eq. 10. In essence, the original area data points (S) were thus compared with pressure points (P') in a linear fashion, as shown by the straightened-out vector plot in Fig. 1 *b*, preserving only the effect of frequency-dependent modulus ratios and phase angle differences.

The linearization technique described here is not exact, but is approximately valid[2] for cases of rather slight nonlinearity (the ordinate of point B falls below the straight line through A and C by 20% or less of the total vertical amplitude), and for rather small phase angles ($\Delta\phi$ at the heart frequency is 10° or less). These conditions were met in all our experiments. The values of the constants k, l, and m are sensitive to the exact placement of point C, but

[2] Some proof of the correctness of the linearization procedure was found as follows. A signal was taken with a 1 s period. A second signal was derived from the first by a quadratic relationship like Eq. 10. The second signal was then delayed with respect to the first by 25 ms, thus artificially creating a "viscous" effect. The two signals were plotted against each other, generating a curved, open, vector loop. Then the linearization procedure was applied as indicated. The resulting constants (k, l, and m) in the nonlinear relationship proved identical to the ones chosen originally, while subsequent Fourier analysis displayed the required phase angle, linearly increasing with frequency at a rate of 9°/Hz, associated with the 25 ms delay.

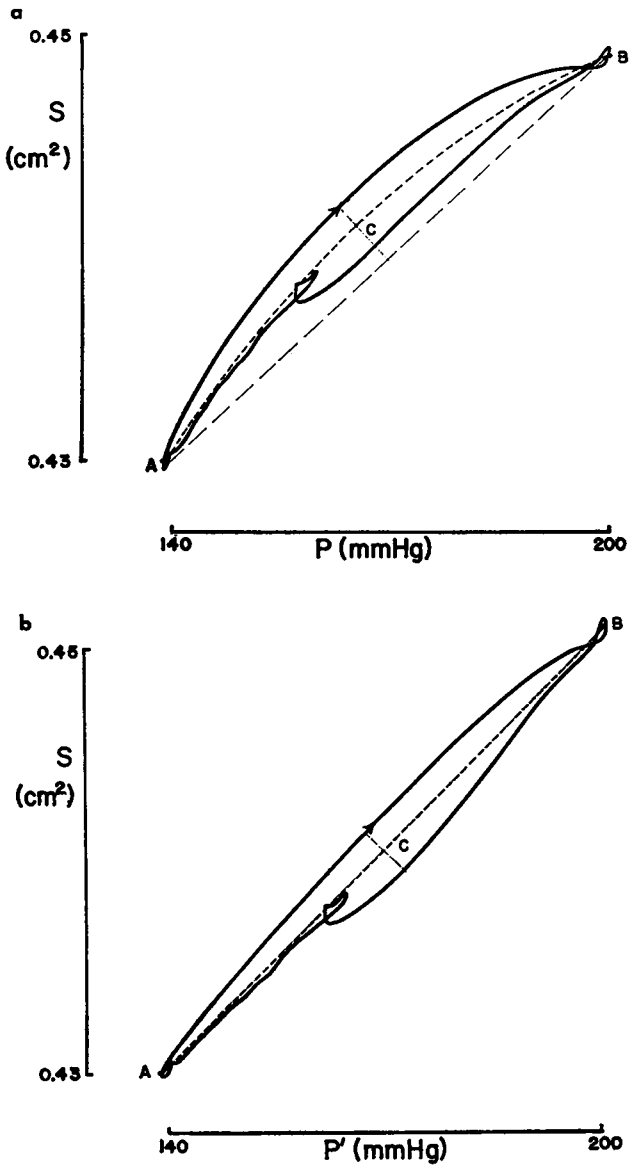

FIGURE 1 (*a*) "Banana-shaped" vector plot of area S vs. pressure P. Dashed line, quadratic curve reflecting nonlinearity alone. (*b*) The same vector plot after straightening out by removal of nonlinearity: area S vs. linearized pressure P'.

the error involved herein was found to be insignificant compared to the standard deviations. A check on the validity of the method consisted in verifying whether a vector plot displaying, e.g., a phase lag of pressure behind area, still showed a phase lag, i.e. a negative phase angle $\Delta\phi$, in the linearized frequency characteristic of inverse distensibility dP'/dS, and vice versa. This invariably proved to be true.

RESULTS

Preliminary data from these experiments were used previously to obtain quasi-static measurements of aortic distensibility and elastic modulus (24). Average values (with standard deviations) for the 11 dogs were: mean pressure, 147 (±20) mmHg; pulsatile pressure, 52 (±17) mmHg; mean internal cross-sectional area, 0.53 (±0.08) cm^2; pulsatile area, 0.04 (±0.016) cm^2; mean internal diameter, 8.2 (±0.63) mm; pulsatile diameter, 0.3 (±0.06) mm; quasi-static inverse distensibility, 2.0 (±0.8) × 10^6 dyn/cm^4; quasi-static elastic modulus, 16 (±5.2) × 10^6 dyn/cm^2.

Phasic Area and Pressure and Vector Plots

Phasic tracings of area and pressure, uncorrected for noise and instrument errors, are shown in Fig. 2 *a*. The phase relationship between the two signals is not easily observed from these records, but manifests itself clearly as a phase lag of area behind pressure in the vector plot shown in Fig. 2 *b*. The results after optical enlargement, retracing and correction for instrument errors are shown for another dog in Fig. 3 *a*. The phase lead of area over pressure in this case is clearly evident in the vector plot printed by the Calcomp plotter shown in Fig. 3 *b*. Notice how even the slight increase in area and pressure accompanying the dicrotic notch reveals the phase lead, a feature obscured by noise and line thickness in unprocessed vector plots.

Effect of Linearization

As evidenced by Figs. 1–3, the vector plots of area vs. pressure were useful not only to reveal phase differences, but also to detect nonlinearity in the relation between area and pressure. The nonlinear effect is strong in Fig. 1 *a* while rather insignificant in Fig. 2 *b*. However, as emphasized previously (12), even a case of slight nonlinearity between two quantities will result in modulus ratios and phase angle differences strongly dependent on frequency when subjected to harmonic analysis. How strong this effect is may be appreciated from Fig. 4 which shows the frequency

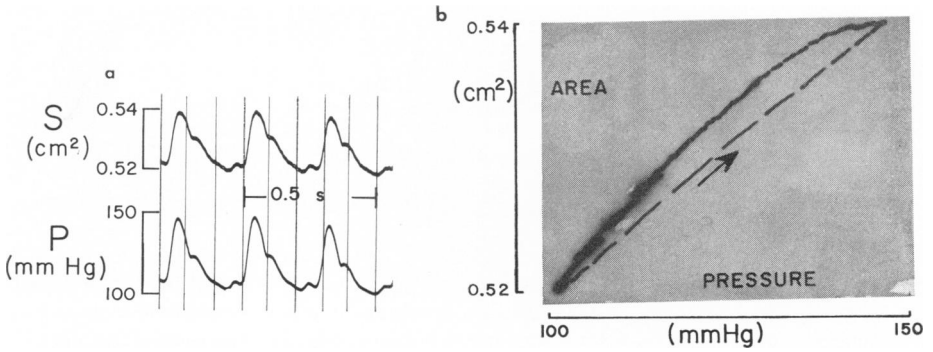

FIGURE 2 (*a*) Area and pressure in the abdominal aorta of dog no. 13 (original data). (*b*) Vector plot of area vs. pressure (original data on *X-Y* recorder). Pressure leads area.

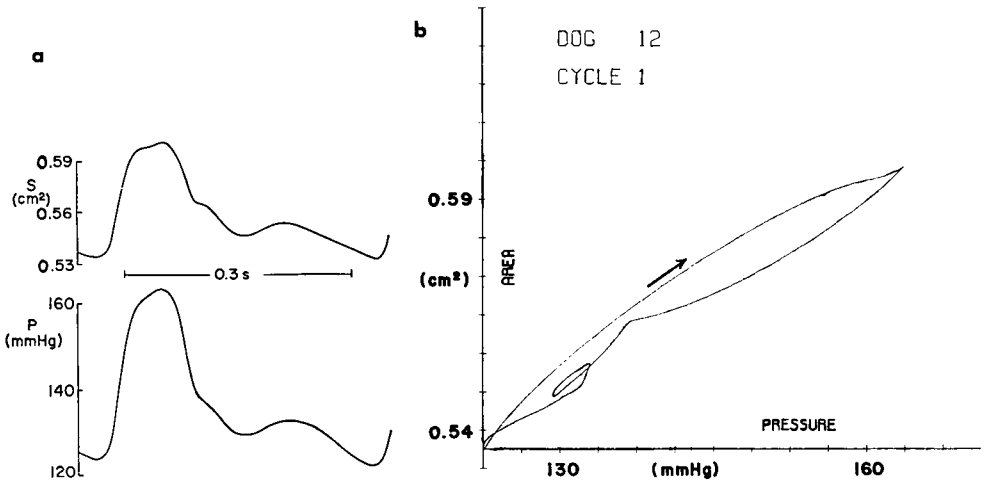

FIGURE 3 (*a*) Area and pressure in the abdominal aorta of dog no. 12 (optically enlarged and retraced data). (*b*) Vector plot of area vs. pressure (data after correction for frequency distortion, as printed by Calcomp plotter). Area leads pressure.

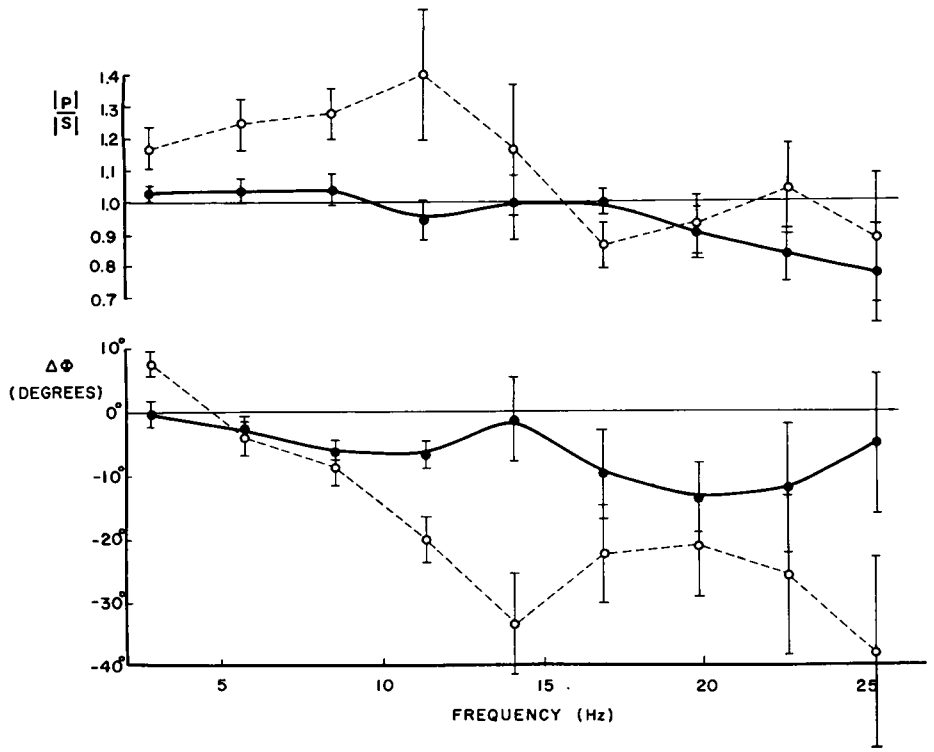

FIGURE 4 Frequency characteristic of inverse distensibility in dog no. 11, showing effect of nonlinearity. *Top:* Modulus ($|P|/|S|$). *Bottom:* Phase angle ($\Delta\phi = \phi_P - \phi_S$). Dashed line, open points: original nonlinear data. Solid line, solid points: after linearization. Vertical bars indicate 2 SD.

characteristics of the inverse distensibility, for both modulus and phase. The dashed lines and open points designate the original, nonlinear data dP/dS, whereas the solid lines and points indicate the results, dP'/dS, after the linearization has been applied. It is seen that both the "jagged" appearance of the modulus plot, $| P/S |$, and the tendency toward strongly negative values in the phase plot, $\Delta\phi$, have been greatly reduced by the linearization. In one case (see below), where the vector plot displayed nonlinearity almost without phase lags (closed vector loop), the linearization procedure indeed reduced the originally substantial phase angles in the frequency characteristic to almost zero.

Axial Motion of the Vessel

The effectiveness of axial tethering of the vessel wall by the surrounding tissue was investigated by recording axial displacement of the wall using the technique described above. These measurements should give a clue as to the validity of the different boundary conditions leading to different theoretical solutions for the local distensibility (Eqs. 7 and 8). Although our method to detect axial motion did not give records as detailed as the area tracings, two cases could easily be discerned: (*a*) Axial motion synchronous with the heartbeat was barely visible, indicating displacements of 0.2 mm or less, as shown in Fig. 5 *a*. (*b*) Axial motion, starting in caudal direction with ventricular systole, was clearly visible and amounted to more than 1 mm, as shown in Fig. 5 *b*.

Displacements coinciding with the respiration (in caudal direction with inspiration) were larger than those synchronous with the heartbeat and were variable: more than 5 mm in Fig. 5 *a*, less than 3 mm in Fig. 5 *b*.

Frequency Characteristics of the Inverse Distensibility

After the linearization procedure had been applied as explained previously, the normalized modulus, $| P'/S |$, and phase angle, $\Delta\phi$, of the inverse distensibility

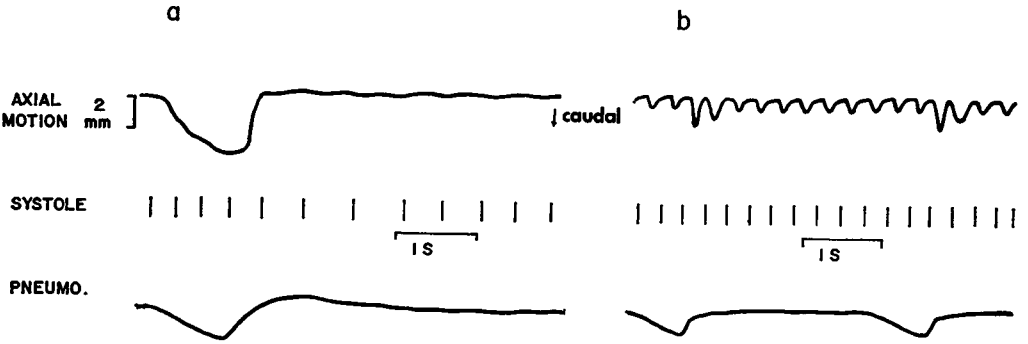

FIGURE 5 *Top:* Axial vessel displacement (optically enlarged and retraced data). *Middle:* Onset of each systole. *Bottom:* Pneumograph tracing. (*a*) Dog no. 7, (group 1): almost no axial displacement (less than 0.2 mm) except during respiratory action. (*b*) Dog no. 6, (group 2): axial displacement of more than 1 mm occurring with each systole and enhanced during expiration.

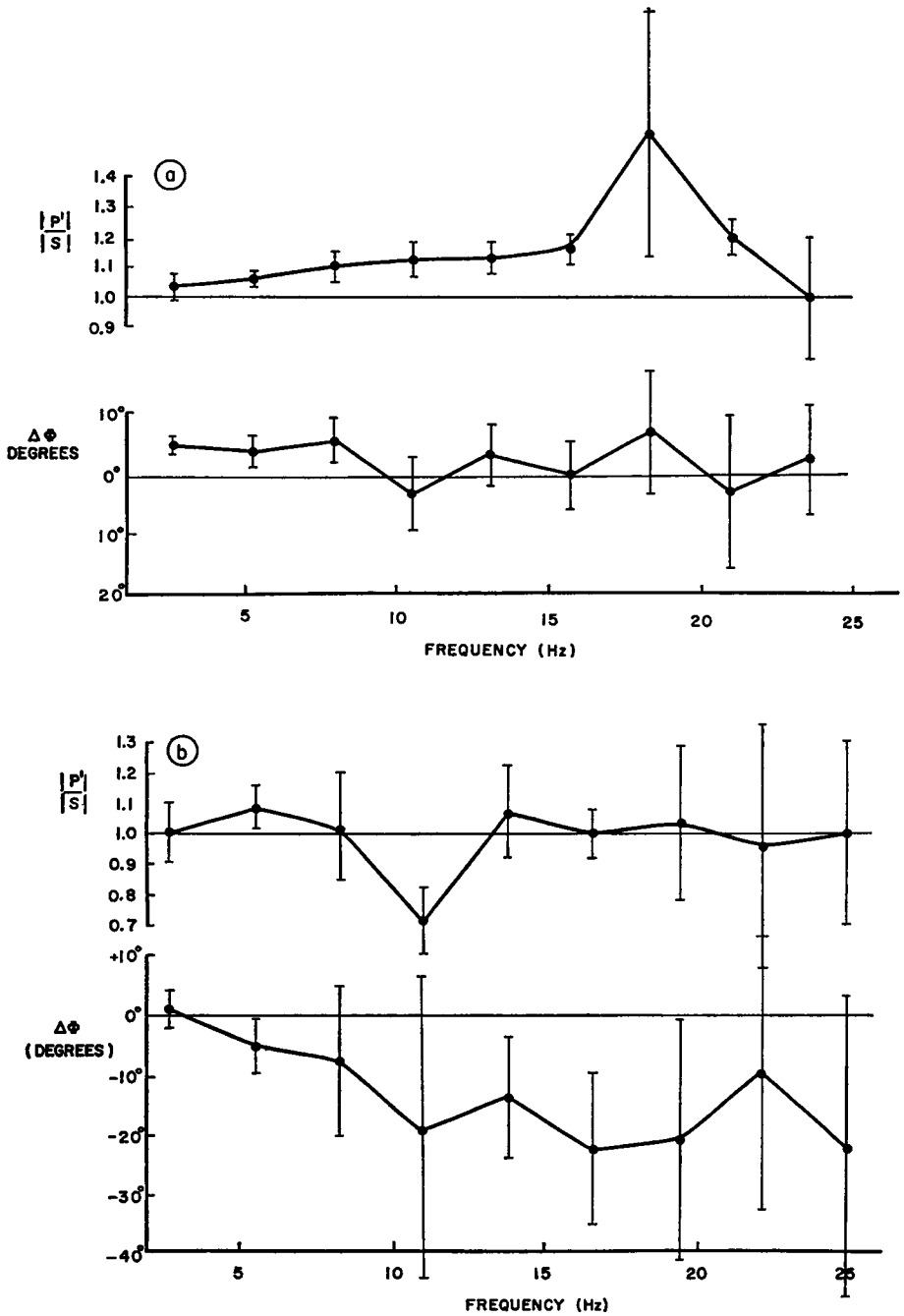

FIGURE 6 Frequency characteristics of linearized inverse distensibility in three dogs. *Top:* Modulus ($|P'|/|S|$). *Bottom:* Phase angle ($\Delta\phi = \phi_{P'} - \phi_S$). Vertical bars indicate 2 SD. (*a*) Dog no. 7, (group 1): pressure leads area. (*b*) Dog no. 12, (group 2): area leads pressure. (*c*) Dog no. 8 (group 3): area and pressure in phase up to 13 Hz.

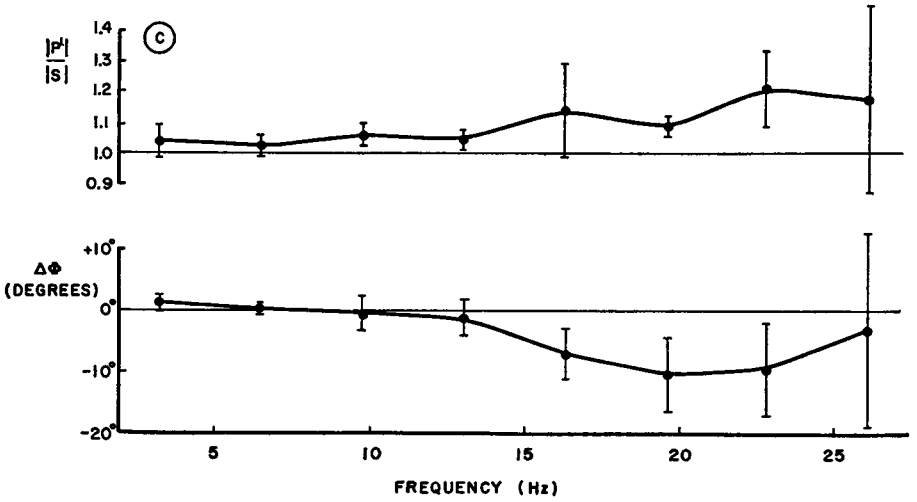

FIGURE 6 c

were plotted against frequency as shown in Figs. 4 and 6. The points represent average values from about 10 heartbeats while the vertical bars indicate 2 SD. The behavior of the frequency characteristic could be classified in one of three categories:

(*1*) The phase angles $\Delta\phi$ were positive, averaging about $+6°$ for frequencies up to 10 Hz, beyond which they fell to zero or to slightly negative values around 15 Hz. The normalized modulus values, $| P'/S |$, were consistently larger than 1 by 10–20% for frequencies up to 15 Hz. An example is given in Fig. 6 *a*. The described behavior was observed in four of the eight analyzed experiments (dogs nos. 7, 9, 10, 13). The positive values for the phase angle at the lower frequencies had been predicted in all of these dogs by the (nonlinear) vector plots of area vs. pressure, exhibiting phase lags of area behind pressure (Fig. 2 *b*). Furthermore, axial motion of the vessel wall in these same experiments was hardly detectable (Fig. 5 *a*).

(*2*) The values of the phase angle $\Delta\phi$ were negative throughout most of the frequency range, being in the order of $-10°$ for frequencies up to 15 Hz. The normalized values for the modulus, $| P'/S |$, averaged around 1. An example is shown in Fig. 6 *b* and also in Fig. 4. These conditions were observed in three of the eight experiments (dogs nos. 6, 11, 12); in each of these three, the negative phase angles had already been apparent from the original (nonlinear) vector plots, which manifested a phase lead of area over pressure (Fig. 3 *b*). In these same dogs, the axial wall motion was clearly visible on the record, amounting to about 1 mm (Fig. 5 *b*).

(*3*) The phase angle $\Delta\phi$ was close to zero for frequencies up to 15 Hz while the normalized amplitude values $| P'/S |$ were slightly (around 5%) larger than 1. This condition was found in only one experiment and is illustrated in Fig. 6 *c*. As mentioned in the Methods section, the zero phase angle had been anticipated by the nonlinear vector plot of area vs. pressure which showed the two to be practically in phase.

The frequency of 15 Hz represents the fifth to sixth harmonic of area and pressure. For higher frequencies the harmonic content of cardiovascular variables rapidly decreases (43), approaching the noise level. Therefore, larger errors should be expected in the higher harmonics of the ratio of the two variables since the percentual errors in each of them have increased. Consequently, a discussion of our data for frequencies above 15 Hz is not necessarily meaningful.

DISCUSSION

The nonlinearity in the relation between area and pressure, observed in most cases, would have been even stronger if radius or diameter were plotted against pressure (sharper curved vector plots). Similar findings have been reported by previous workers, most notably by Bergel (26, 27), who interpreted and quantified this phenomenon as an increase in the wall's Young's modulus (E^*) with increasing stress, using an equivalent form of Eq. 7. Our data, no matter whether area variations lead or lag pressure variations, generally support his conclusions. However, quantification of the stress dependence of E^* is impossible for the case when axial motion is present, so long as a static equivalent of Eq. 8 is lacking.

Our finding that in the lower abdominal aorta of radial extensions (cross-sectional area) lagged pressure variations in phase in about half the cases, while in the other half the reverse situation was obtained, is not easily explained. Instrumental errors can be safely excluded. The amount of dissection of perivascular tissue (more extensive for the two experiments in which a flow probe was placed) does not give a clue either. In fact, when a large amount of tissue was dissected in one experiment to investigate the specific peculiarities of the phase relationship and the axial vessel motion, no changes in the behavior of these quantities could be detected when comparing data before and after the dissection. Other investigators also have observed the phenomenon of positive and negative values for the phase of the distensibility, especially when measuring in the aorta (9, 10, 12, 30). Our observations of the axial wall motion, however, may shed some light on the situation. Previous workers have measured axial wall strains, finding these to be quite dominant in the aortic arch (31), but less significant in the descending aorta (32). Quite often, these axial strains were felt to account for the phase leads of radial extensions over pressure variations (31, 32). That this indeed may be the case is best explained in terms of energy (32), as follows:

The net energy per unit length, W, spent on radially moving the wall during one cycle T, is given by a closed path integral:

$$W = \oint_T P dS. \tag{11}$$

For the simple case in which area (S) and pressure (P) are in phase, (purely elastic wall), this energy equals zero. In the case in which pressure leads area in phase, W is

positive and amounts to the viscous energy loss (heat) in the wall, per cycle and per unit length. This phenomenon is called mechanical hysteresis. In a transmission line model of an arterial segment, W corresponds to the heat loss through the resistive components of the transverse impedance (38, 44). In the third case, in which area leads pressure in phase, a negative value for W in Eq. 11 will result. This phenomenon has previously been termed "energy gain" by the vessel wall (4), or "negative viscosity" (45), or, in transmission line analogy, "negative resistance" (44). However, referring back to the Introduction, above, it is evident that the definition of W in Eq. 11 is valid only for vessel segments of fixed length. If allowance is made for imperfect or absent axial tethering by perivascular tissue, axial forces will cause the length to vary and the new expression for energy spent on the wall per unit length and per cycle becomes:

$$W = (1/\bar{L}) \oint_T P d(SL) = \oint_T P dS + (\bar{S}/\bar{L}) \oint_T P dL \qquad (12)$$

where the dash over a symbol indicates its mean value during the cycle. (This equation is valid in good approximation, since the variations during one cycle in both S and L are small). It is clear now that a negative value for the first term on the right-hand side of Eq. 12, combined with a positive value for the second term, could very well result in a zero or even positive value for W. Thus we see that axial strains (dL) can indeed account for negative values of the term $\oint PdS$, associated with phase leads of area over pressure. Moreover, the above consideration of energy compels one to broaden the definition of local vessel distensibility. Per unit length, this quantity has two components: a radial, dS/dP, and an axial component, $(\bar{S}/\bar{L})\ dL/dP$. Studies in vivo of the quantity dL/dP have so far been indirect (46, 47).

The present study deals strictly with the quantity dS/dP, but the experimental results will be discussed in connection with our findings for the axial displacements of the vessel wall which are very helpful in explaining the data in terms of the theoretically predicted behavior of the (radial) distensibility. The three groups mentioned above in the Results section and distinguished by the sign of the phase angle, are discussed separately.

(*1*) Phase angle positive or pressure leads area; no noticeable axial motion. Our findings for the phase angle in these experiments (around $+6°$ for frequencies below 10–15 Hz) match, on the average, those obtained by other investigators, mostly measured in vitro. Their results have been summarized by Westerhof et al. (38), who reports an average value for $\Delta\phi$ of $+6°$ between 1 and 10 Hz. The average values for the modulus, $| P'/S | > 1$ for all frequencies, also match those found by others (38), though to a lesser extent. The extremely small amplitude of the axial wall motion in these cases could, in fact, be entirely ballistocardiographic in origin (48), thus implying no relative motion between vessel and body. Therefore, a comparison

of the distensibility results in this group to the theoretical solution for dS/dP, in which infinitely strong axial tethering was a boundary condition, appears warranted. In this formula (Eq. 7), the only frequency dependent variable is the complex Young's modulus, $E^*(\omega)$. Indeed, a positive value for $\Delta\phi$ in the frequency characteristic of dP/dS reflects a positive value for the phase angle of E^* and indicates the presence of a viscous component in the elastic modulus (real part: elastic; imaginary part: viscous; both positive). Thus the validity of the boundary condition of strong axial tethering which led to the (dynamic) formula in Eq. 7 has now been proven experimentally in these cases. Another cause for positive values of $\Delta\phi$ would reside in the inertial effect of the mass of the wall and surrounding tissue. However, this effect has been shown to be negligible (38).

(*2*) Phase angle negative or area leads pressure; easily observed axial motion. Results like these have never been found in vitro but nevertheless have a ready possible physical explanation as outlined above. The appreciable axial motion of the wall warrants a comparison of the experimental findings in this group to the wave transmission solution for dS/dP in which absence of axial tethering was a boundary condition. When plotting the phase angle of the inverse of the derived relationship (Eq. 8) against frequency, a picture resulted as shown in Fig. 7. Here, the appropriate values for the lower abdominal aorta were substituted: internal radius $a = 0.4$ cm, wall thickness ratio $h = 0.12$. In order not to obscure the picture, Young's modulus E was taken as a real quantity, representing a purely elastic wall. (If viscosity is taken into account, the effect would be to add about 6° to the predicted phase angles for all frequencies). The figure shows that the predicted phase angles are negative, signifying a phase lead of area over pressure, just as found experimentally. The predicted order of magnitude of $\Delta\phi$ is also right, namely from $-20°$ to 0°; experimental values were in the neighborhood of $-10°$ (Figs. 4 and 6 *b*). However, the frequency range where the predicted phase angles occur does not match the experimental findings, since the former lie mainly in the range below 3 Hz whereas the observed values for $\Delta\phi$ appear to increase with frequency above 3 Hz (Figs. 4 and 6 *b*). Gross mistakes in the derivation of Eq. 8 are very unlikely, since the values

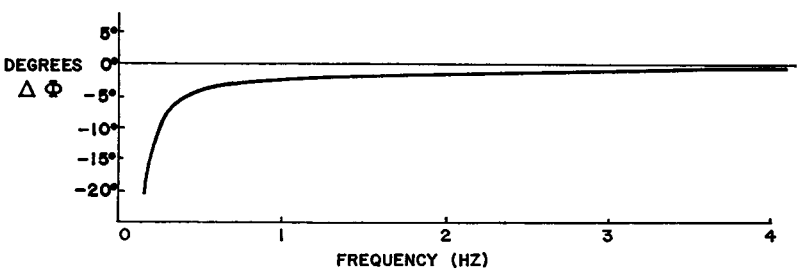

FIGURE 7 Theoretically predicted phase angle of inverse distensibility as a function of frequency, for a thick-walled elastic tube similar to the abdominal aorta, allowed to move freely in axial direction (Eq. 8).

shown in Fig. 7 are numerically close to those given for the phase angle by Womersley (42) who derived his solutions in a totally different fashion and for the relatively simple case of a thin-walled elastic tube.

We must, therefore, conclude that the case of phase leads of area over pressure can be partially explained by wave transmission theory in which allowance was made for the wall to move in axial direction. It is remarkable that sign and rough magnitude of the phase angle are correctly predicted, but the mismatch of the frequency ranges is indicative of some shortcomings in the theoretical treatment. Indeed, the only axial force considered in the equations of motion is the force exerted by the viscous drag of the blood at the wall interface (23). The fact that the phase leads of radial extensions over pressure were found to be large near the heart (4, 31), moderate in the thoracic aorta (12, 32), occasionally occurring in the abdominal aorta (32, this study) and absent in the femoral artery (5, 12, 31), leads us to suspect that other forces must be operative. These forces could include inertial effects of the heart's motion, transmitted via an imperfectly tethered aorta, bending forces of the aortic arch, variable coupling of the aorta to the diaphragm, etc. Our finding that an increased removal of perivascular tissue did not seem to influence the results lends strong support to the assumption of the presence of additional forces. In addition, nonisotropic elastic properties of the wall (47), which is considered isotropic in the theoretical treatments, may play a role in the observed behavior.

(*3*) Phase angle zero, or area and pressure are in phase. After the discussion of the previous two cases, it is clear that this phenomenon could indicate a purely elastic wall, but just as likely, perhaps, have the effects of viscoelasticity (positive $\Delta\phi$) and of axial motion (negative $\Delta\phi$) cancelled each other to give a phase angle of approximately zero. The lack of sensitivity in the axial motion recording precluded confirmation of this supposition.

In summary, having studied the frequency dependence of the local arterial distensibility in the living animal, along with the recording of axial wall motions, and having placed the results in the perspective of arterial wave transmission theory, has led to several important conclusions. When axial displacements are virtually absent, the theory assuming constant vessel length correctly predicts the frequency dependent behavior of the distensibility, displaying positive phase angles for frequencies up to 10 Hz, which can numerically be related to the phase angles of the viscoelastic Young's modulus of the vessel wall. Thus, under these circumstances, reliable information about the wall properties in vitro can indeed be obtained from measurements in vivo. If, on the other hand, axial wall displacements are prominent, the frequency dependent distensibility data, displaying negative phase angles for most frequencies, can fruitfully be compared with the theory which assumes freedom of the vessel wall to move in axial direction. This comparison is successful to a certain extent, but the theoretical formula is not good enough yet to be useful in a sense that it can be applied as a correction term to account for the disturbing effect of axial motion. Therefore, under these circumstances, one cannot draw conclusions re-

garding the frequency dependent viscoelastic properties of the isolated wall. However, the results do indicate a more complex behavior of the living aortic configuration, warranting a search for improvements to the theory combined with the dynamic recording of more experimental variables.

LIST OF SYMBOLS

a Internal vessel radius.
c Phase velocity.
E Young's modulus.
E^* Complex Young's modulus.

$$F_{10} = \frac{2J_1(\alpha_w j^{3/2})}{\alpha_w j^{3/2} J_0(\alpha_w j^{3/2})}$$

$$g(F_{10}) = \frac{4 - F_{10} + \{(4 - F_{10})^2 - 12[h(2 + h)/(1 + h)^2] \cdot (1 - F_{10})(1 - [F_{10}/h(2 + h)])\}^{\frac{1}{2}}}{6(1 - F_{10})}$$

h Ratio of wall thickness over internal radius.
j Imaginary unity.
J_0, J_1 Bessel functions of order 0 and 1.
k, l, m Constants in nonlinear pressure equation.
L Vessel segment length.
P Pressure.
$|P|$ Modulus of pressure harmonic.
P' Linearized pressure $= kP^2 + lP + m$.
Q Flow.
S Internal cross-sectional area.
$|S|$ Modulus of area harmonic.
T Period of 1 cycle.
t Time.
W Energy spent on moving wall per unit length and per cycle.
Y_t Transverse admittance per unit length.
Z_l Longitudinal impedance per unit length.
Z_t Transverse impendance $= 1/Y_t$.
Z_0 Characteristic impedance $= \sqrt{Z_l Z_t}$.
Z_i Input impedance.
z Longitudinal coordinate.
α Attenuation coefficient.
α_w Dimensionless frequency parameter $= a\sqrt{\omega/\nu}$.
β Wave number $= \omega/c$.
γ Propagation constant $= \sqrt{Z_l/Z_t}$.

ν	Kinematic fluid viscosity.
π	3.14.
ϕ_P	Phase angle of pressure harmonic.
ϕ_S	Phase angle of area harmonic.
$\Delta\phi$	Phase angle of inverse distensibility $= \phi_P - \phi_S$. .
ω	Circular frequency.

The authors are grateful to Dr. Alfred P. Fishman, Director of the Cardiovascular-Pulmonary Division, for making this study possible and for counsel, encouragement and critical review during its course. They are also indebted to Mrs. Ineke Baan for helping with the vast amount of data analysis. This study was supported by National Heart and Lung Institute grants HE-08805, HE-05896, and HE-10330.

Received for publication 19 September 1973.

REFERENCES

1. CAREW, T. E., R. N. VAISHNAV, and D. J. PATEL. 1968. *Circ. Res.* **23**:61.
2. LOVE, A. E. H. 1944. A Treatise on the Mathematical Theory of Elasticity. Dover Publications Inc., New York. 4th edition.
3. RUSHMER, R. F., R. M. ELLIS, A. A. NASH, and B. L. FINLAYSON. 1954. *Fed. Proc.* **13**:123.
4. RUSHMER, R. F. 1955. *Am. J. Physiol.* **183**:545.
5. PARRISH, D., D. E. STRANDNESS, JR., and J. W. BELL. 1964. *J. Appl. Physiol.* **19**:363.
6. LAWTON, R. W. 1955. *Circ. Res.* **3**:403.
7. PATEL, D. J., D. P. SCHILDER, and A. J. MALLOS. 1960. *J. Appl. Physiol.* **15**:92.
8. MALLOS, A. J. 1962. *J. Appl. Physiol.* **17**:131.
9. BARNETT, G. O., A. J. MALLOS, and A. SHAPIRO. 1961. *J. Appl. Physiol.* **16**:545.
10. REMINGTON, J. W. 1962. *Am. J. Physiol.* **203**:440.
11. GOW, B. S. 1966. *J. Appl. Physiol.* **21**:1122.
12. GOW, B. S., and M. G. TAYLOR. 1968. *Circ. Res.* **23**:111.
13. PETERSON, L. H., R. JENSEN, and J. PARNELL. 1960. *Circ. Res.* **8**:622.
14. PETERSON, L. H. 1966. *In* Methods in Medical Research. Vol. 11. R. F. Rushmer, editor. Year Book Medical Publishers, Inc., Chicago.
15. COX, R. H. 1967. Wave propagation through a Newtonian fluid contained within a thick-walled viscoelastic tube: a model for arterial blood flow. Doctoral Dissertation. University Microfilms, Ann Arbor, Mich.
16. KATZ, L. N., M. R. MALINOW, B. KONDO, D. FELDMAN, and N. GROSSMAN. 1947. *Am. Heart J.* **33**:319.
17. EVANS, R. L., E. F. BERNSTEIN, E. JOHNSON, and C. RELLER. 1962. *Am. J. Physiol.* **202**:619.
18. LUCHSINGER, P. C., M. SACHS, and D. J. PATEL. 1962. *Circ. Res.* **11**:885.
19. LEAROYD, B. M., and M. G. TAYLOR. 1966. *Circ. Res.* **10**:278.
20. GARDNER, R. M., and H. R. WARNER. 1967. *Comput. Biomed. Res.* **1**:50.
21. ARNDT, J. O., J. KLAUSKE, and F. MERSCH. 1968. *Pflügers Arch.* **301**:230.
22. KOLIN, A., and G. W. CULP. 1971. *IEEE Trans. Bio-med. Eng.* **18**:110.
23. BAAN, J. 1970. Transverse impedance of arteries: animal experiments related to wave transmission theory. Doctoral Dissertation. University Microfilms, Ann Arbor, Mich.
24. BAAN, J., T. IWAZUMI, J. P. SZIDON, and A. NOORDERGRAAF. 1971. *J. Appl. Physiol.* **31**:499.
25. HARDUNG, V. 1953. *Helv. Physiol. Pharmacol. Acta.* **11**:194.
26. BERGEL, D. H. 1961. *J. Physiol.* **156**:445.
27. BERGEL, D. H. 1961. *J. Physiol.* **156**:458.
28. LAIRD, J. D., and P. N. MADRAS. 1969. Proceedings of the 8th International Conference on Engineering in Medicine and Biology, Chicago. 18-8.

29. OKINO, M., and F. SANO. 1969. Proceedings of the 8th International Conference of Engineering in Medicine and Biology, Chicago. 18-6.
30. PATEL, D. J., and W. G. AUSTEN. 1964. *Ann. N. Y. Acad. Sci.* **115**:1129.
31. VAN CITTERS, R. L., and R. F. RUSHMER. 1961. *Am. J. Physiol.* **200**:732.
32. PATEL, D. J., A. J. MALLOS, and D. L. FRY. 1961. *J. Appl. Physiol.* **16**:293.
33. NOORDERGRAAF, A. 1969. *In* Biological Engineering. H. P. Schwan, editor. McGraw-Hill, Inc., New York.
34. JAGER, G. N., N. WESTERHOF and A. NOORDERGRAAF. 1965. *Circ. Res.* **16**:121.
35. JAGER, G. N. 1965. Electrical model of the human systemic arterial tree. Doctoral Dissertation. Elinkwijk Press, Utrecht.
36. TAYLOR, M. G. 1966. *Biophys. J.* **6**:697.
37. ATTINGER, E. O., and A. ANNE. 1966. *Ann. N. Y. Acad. Sci.* **128**:810.
38. WESTERHOF, N., F. BOSMAN, C. J. DEVRIES, and A. NOORDERGRAAF. 1969. *J. Biomech.* **2**:121.
39. WOMERSLEY, J. R. 1955. *J. Physiol.* **127**:553.
40. WITZIG, K. 1914. Ueber erzwungene Wellenbewegungen zäher, inkompressibler Flüssigkeiten in elastischen Röhren. Inaugural Dissertation, University of Bern, Bern.
41. COX, R. H. 1968. *Biophys. J.* **8**:691.
42. WOMERSLEY, J. R. 1957. An elastic tube theory of pulse transmission and oscillatory flow in mammalian arteries. Wright Air Development Center Tech. Rep. TR56-614.
43. ATTINGER, E. O., A. ANNE, and D. A. MCDONALD. 1966. *Biophys. J.* **6**:291.
44. TAYLOR, M. G. 1959. *Phys. Med. Biol.* **4**:63.
45. HARDUNG, V. 1962. *Handb. Physiol. Sect.* 2. **1**:107.
46. PATEL, D. J., and D. L. FRY. 1966. *Circ. Res.* **19**:1011.
47. PATEL, D. J., J. S. JANICKI, and T. E. CAREW. 1969. *Circ. Res.* **25**:765.
48. STARR, I., and A. NOORDERGRAAF. 1967. Ballistocardiography in Cardiovascular Research. J. B. Lippincott Company, Philadelphia.